To be published in *Supercollider 4* SSCL-Preprint-82

Review of SSC Dipole Magnet Mechanics and Quench Performance*

A. Devred, et al.

Superconducting Super Collider Laboratory †
2550 Beckleymeade Ave.
Dallas, TX 75237

March 1992

---

*Presented at the International Industrial Symposium on the Super Colider, New Orleans, March 4-6, 1992.

† Operated by the Universities Research Association, Inc., for the U.S. Department of Energy under Contract No. DE-AC35-89ER40486.

REVIEW OF SSC DIPOLE MAGNET MECHANICS AND QUENCH PERFORMANCE*

A. Devred, T. Bush, R. Coombes, J. DiMarco, C. Goodzeit, J. Kuzminski, W. Nah, T. Ogitsu, M. Puglisi, P. Radusewicz, P. Sanger, R. Schermer, R. Stiening, G. Spigo, J. Tompkins, J. Turner, Y. Yu, Y. Zhao, and H. Zheng

Magnet Systems Division
Superconducting Super Collider Laboratory
2550 Beckleymeade Avenue
Dallas, TX 75237 USA

M. Anerella, J. Cottingham, G. Ganetis, M. Garber, A. Ghosh, A. Greene, R. Gupta, A. Jain, S. Kahn, E. Kelly, G. Morgan, J. Muratore, A. Prodell, M. Rehak, E. P. Rohrer, W. Sampson, R. Shutt, R. Thomas, P. Thompson, P. Wanderer, and E. Willen

Brookhaven National Laboratory, Upton, NY 11973 USA

M. Bleadon, R. Bossert, J. Carson, S. Delchamps, S. Gourlay, R. Hanft, W. Koska, M. Kuchnir, M. Lamm, P. Mantsch, P. O. Mazur, D. Orris, J. Ozelis, T. Peterson, J. Strait, and M. Wake

Fermi National Accelerator Laboratory, Batavia, IL 60510 USA

J. Royet, R. Scanlan, and C. Taylor

Lawrence Berkeley Laboratory, Berkeley, CA 94720 USA

ABSTRACT

Eight 5-cm-aperture, 15-m-long dipole magnet prototypes have been produced and cold-tested at Brookhaven National Laboratory (BNL) and Fermi National Accelerator Laboratory (FNAL) under contract with the Superconducting Super Collider Laboratory (SSCL). These magnets are the last phase of an R&D program aimed at demonstrating the feasibility of the 5-cm-aperture designs developed by BNL and FNAL. They are also used

* This work is supported by the U.S. Department of Energy under contract No. DE-AC35-89ER40486.

as vehicles to transfer technology from the National Laboratories to the collider dipole magnet contractors. The BNL magnets, which rely on an horizontally-split yoke, and the FNAL magnets, which rely on a vertically-split yoke, perform according to their somewhat different mechanical designs and have equally successful quench performance.

INTRODUCTION

In January 1990, the decision was taken to increase the aperture of the Superconducting Super Collider (SSC) dipole magnets from 4 cm[1] to 5 cm[2] in order to improve the field quality and reduce the risk of beam losses.[3] A large effort was then started at Brookhaven National Laboratory (BNL) and Fermi National Accelerator Laboratory (FNAL) to design and build 5-cm-aperture dipole magnet prototypes. The first short model magnet of the BNL 5-cm-aperture design was produced by KEK, National Laboratory for High Energy Physics, in the summer of 1990.[4] It was soon followed by a series of 1.8-m-long model magnets at BNL[5] and a series of 1.5-m-long model magnets at FNAL.[6] In the fall of 1991, BNL and FNAL completed the production of their first 5-cm-aperture, 15-m-long dipole magnet prototypes. Thus far, three full-length prototypes of the BNL design (magnets DCA207, DCA208, and DCA209) have been built and cold-tested at BNL, and five full-length prototypes of the FNAL design (magnets DCA311, DCA312, DCA313, DCA314, and DCA315) have been built and cold-tested at FNAL.

The main goals of the 5-cm-aperture dipole magnet R&D program are to demonstrate the feasibility of the larger-aperture magnets and to provide to the collider dipole magnet contractors a basis on which to start their design efforts. The production of the full-length prototypes is also used as a vehicle to transfer technology from the National Laboratories to the magnet contractors. Three of the FNAL-design magnets (magnets DCA313, DCA314, and DCA315) were assembled by personnel from General Dynamics, and one of the BNL-design magnets (magnet DCA209) was assembled by personnel from Westinghouse Electric Corporation. General Dynamics is the leader of the collider dipole magnet contract and is expected to assemble seven dipole magnet prototypes at FNAL. Westinghouse is the follower of the dipole magnet contract and is expected to assemble five prototypes at BNL. Five of these ten industrially-assembled prototypes will be used in a string test to be performed at the SSCL by the end of 1992.

The BNL and FNAL 5-cm-aperture designs are scale-ups of the 4-cm-aperture designs previously developed. Both designs use a common magnetic cross section.[7] They rely on similar mechanical concepts, inherited from the 4-cm-aperture dipole magnet R&D program,[8-10] but they differ in the way these concepts are implemented. The main difference is the orientation of the yoke split. The yoke of the BNL magnets is split horizontally, while that of the FNAL magnets is split vertically.[11] In the first section of this paper, we shall detail the key features of the two mechanical designs, and we shall explain their rationale. In the second section, we shall review the mechanical behavior of the eight full-length prototypes during cold-testing, and we shall discuss how the behavior conforms to the two different designs. The last two sections will be devoted to quench performance and ramp-rate sensitivity. Additional information on the assembly of these prototypes are presented in References 12 and 13, while preliminary reports on their field quality can be found in References 14 and 15.

MAGNET FEATURES

Design Concepts

The required field of 6.6 T at 6500 A is produced by a two-layer cosine-theta coil.[7] The inner layer contains 19 turns and 3 copper wedges, and it is wound from a 1.2° keystone-angle cable of 30 strands (strand diameter 0.808 mm). The outer layer contains 26 turns and 1 copper wedge, and it is wound from a 1.05° keystone-angle cable of 36 strands (strand diameter 0.648 mm). The cable insulation consists of a 25.4-μm-thick layer of Kapton®,* wrapped with a 50% overlap, completed by a 9-mm-wide, 102-to-127-μm-thick layer of epoxy-impregnated fiberglass, wrapped with a 0.5-mm gap.

The coil is mechanically restrained by means of laminated stainless steel collars. The 1.5-mm-thick collar laminations are spot-welded by pairs and stacked into packs. The packs are locked around the coil by means of four tapered keys,[16] which are driven horizontally into the keyways near the midplane. The collars are designed to pre-compress the coil azimuthally. The level of pre-compression is determined in order to compensate three effects:[10] 1) stress relaxation during assembly, attributed to insulation flow or creep, 2) stress loss during cooldown, due to thermal shrinkage differentials between the various parts, and 3) stress redistribution during excitation, mainly due to the azimuthal component of the Lorentz force. The target pre-compressions at room temperature are 70 MPa for the coil inner layer, and 55 MPa for the coil outer layer.

The magnet cold mass is completed by a laminated iron yoke and a 4.95-mm-thick stainless steel outer shell. The iron yoke surrounds the collars and enhances the magnetic field by roughly 20%. The outer shell is welded around the yoke and delimits the region of circulation for the 4.35-K, 0.4-MPa forced flow of supercritical helium. Yoke and shell are designed to tightly clamp the collared-coil assembly and to stiffen the support against the radial and axial components of the Lorentz force. The yoke support is needed to limit the collar deflections along the horizontal diameter, where the effect of the radial component of the Lorentz force is largest. The yoke clamping also allows, toward the magnet ends, distribution of the axial component of the Lorentz force between the collared-coil assembly, the yoke, and the outer shell.

The coil is loaded axially at both extremities by means of four screws. The screws are mounted in thick stainless steel end plates, which are anchored to the outer shell. The axial loading allows tight compaction of the coil ends and increases their stiffness. It is also needed to support the fraction of the axial component of the Lorentz force that is not transmitted to the yoke and the outer shell, and to prevent stick-slip motions of the laminated collared-coil assembly inside the laminated yoke.

BNL Design

Figure 1(a) displays a cross-sectional view of the BNL 5-cm-aperture dipole magnet design. The key features of the BNL design are horizontally-split yoke and anti-ovalized, stainless steel collars. The inner boundary of the horizontally-split yoke is a circle with a radius of 67.82 mm. The inner and outer boundaries of the anti-ovalized collars are circular, and their centers coincide. The collars' outer radius is the same as the yoke's inner radius. However, the keyways at the collars' midplane are placed asymmetrically so that when the top and bottom collars are joined and keyed (with no coil in them), the center of the top collars is shifted downward along the vertical axis by 0.10 mm with respect to the center of the bottom collars. As a result, the vertical outer diameter of the keyed collars (with no coil in them) is 0.10 mm smaller than the yoke inner diameter, while the horizontal diameters are the same.

---

* Kapton® is a registered trademark of E.I. DuPont de Nemours & Co.

The rationale behind the BNL design is as follows. During collaring, the coil is squeezed into the collars with a large azimuthal pre-compression. After collaring, the coil exerts a large pressure against the collar poles. This internal pressure causes a large outward deflection of the collared-coil assembly along the vertical diameter and a slight inward deflection along the horizontal diameter. The slight inward deflection allows assembly of the horizontally-split yoke around the collared coil. The large outward vertical deflection is partially compensated by the fact that the collars are anti-ovalized, but it can result in a gap between the two yoke halves. During welding of the outer shell, the shell is put into tension, compressing the yoke. The yoke, in turn, compresses the collared-coil assembly, and the eventual gap between the two yoke halves closes. At the end of shell welding, the yoke gap is closed, and the outer circumference of the collared-coil assembly fits perfectly to the inner circumference of the yoke.

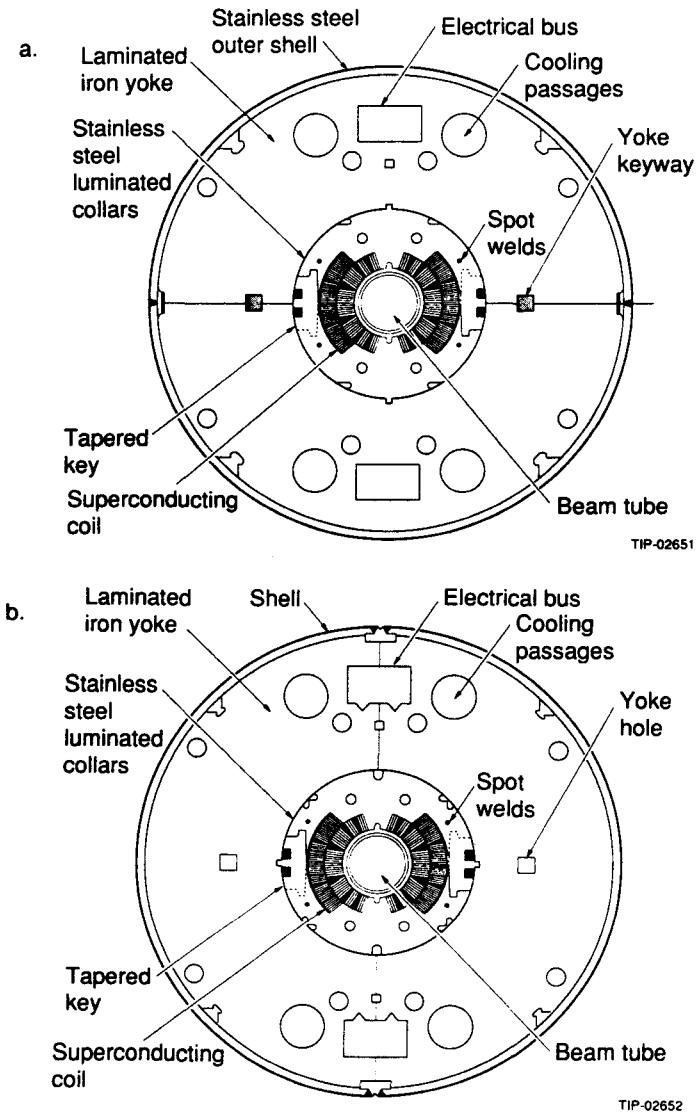

Figure 1. Cross sectional view of the cold mass of 5-cm-aperture, 15-m-long dipole magnet prototype: (a) BNL, horizontally-split yoke, and (b) FNAL, vertically-split yoke dipole magnet designs.

During cooldown, the coil shrinks more than the Nitronic-40 stainless steel collars, which, in turn, shrink more than the low-carbon steel yoke. The pressure exerted by the coil against the collar poles decreases, but it remains large enough to keep deflecting the collars and to maintain contact with the yoke along the vertical diameter. Along the horizontal diameter, however, the thermal shrinkage differentials result in a small gap between the collared-coil assembly and the yoke.

During excitation, the azimuthal component of the Lorentz force causes a redistribution of the coil stress, resulting in a decrease of the pressure exerted by the coil against the collar poles. At the same time, the radial component of the Lorentz force causes a bending of the collars—with a maximum displacement along the horizontal diameter—at the location of the gap between the collared-coil assembly and the yoke. As the current increases, the bending moment increases, and the collars keep deflecting along the horizontal diameter until they come into contact with the yoke. At high currents, the collared-coil assembly touches the yoke on a large perimeter on both sides of the horizontal plane, and the yoke provides an extremely stiff support against the radial component of the Lorentz force.

The diameter reduction of the anti-ovalized collars along the vertical axis is determined in order to ensure that on one hand, at the end of shell welding, the gap between the two yoke halves is closed, and that on the other hand, at the end of cooldown, there remains a suitable interference between the collared-coil assembly and the yoke. The amount of vertical collar-yoke interference at liquid helium temperature is determined in order to ensure that during excitation the current at which the collared-coil assembly comes into contact with the yoke along the horizontal diameter is well below the operating current. Table 1 summarizes the estimated vertical collar-yoke interference at room temperature for the three BNL magnets considered in this paper. The estimates, based on measurements of the collared-coil assembly diameters, assume that the yoke midplane gap is closed. The room-temperature interference appears to be of the order of 170 μm along the vertical diameter.

As we described, the BNL design does not have a built-in collar-yoke interference, but relies on deformations of the collared-coil assembly to seek out the yoke support. The absence of a built-in interference results in a somewhat loose clamping of the collared-coil assembly by the yoke, and toward the magnet ends only a small fraction of the axial component of the Lorentz force can be transmitted to the yoke and the outer shell. In order to increase the rigidity of the coil ends, the coil axial pre-load is setup to a high value of the order of 50 kN.

Other specific features of the BNL design include internal splices between the inner and outer layer conductors, located at the radius of the coil outer layer. As displayed in Figure 2(a), the coil ends are supported by means of stainless steel collars, similar to the case of the magnet body, except for the pole parts. The BNL magnets also integrate an improved cooling scheme, known as cross-flow cooling,[17] which involves the radial circulation of helium at set intervals along the magnet length, from the yoke cooling passages to the coil cooling passage.

Table 1. Estimated room-temperature collar-yoke interference on selected 5-cm-aperture, 15-m-long collider dipole magnet prototypes. The estimates are based on measurements of the collared-coil assembly diameters. The quoted values refer to the vertical diameter for the BNL magnets and to the horizontal diameter for the FNAL magnets.

	DCA207	DCA208	DCA209	DCA311	DCA312	DCA313	DCA314	DCA315
At Lead-End Strain-Gauge Pack	153	179	154	305	318	318	288	263
At Non-Lead-End Strain-Gauge Pack	n/a	n/a	n/a	305	318	330	300	275
In Average Over Magnet Length[a]	170 (28)	167 (32)	162 (19)	330 (20)	340 (15)	335 (18)	290 (25)	285 (20)

[a] The number and the number in parentheses correspond respectively to the mean and the standard deviation. For DCA2XX magnets, the end-collars are not taken into account.

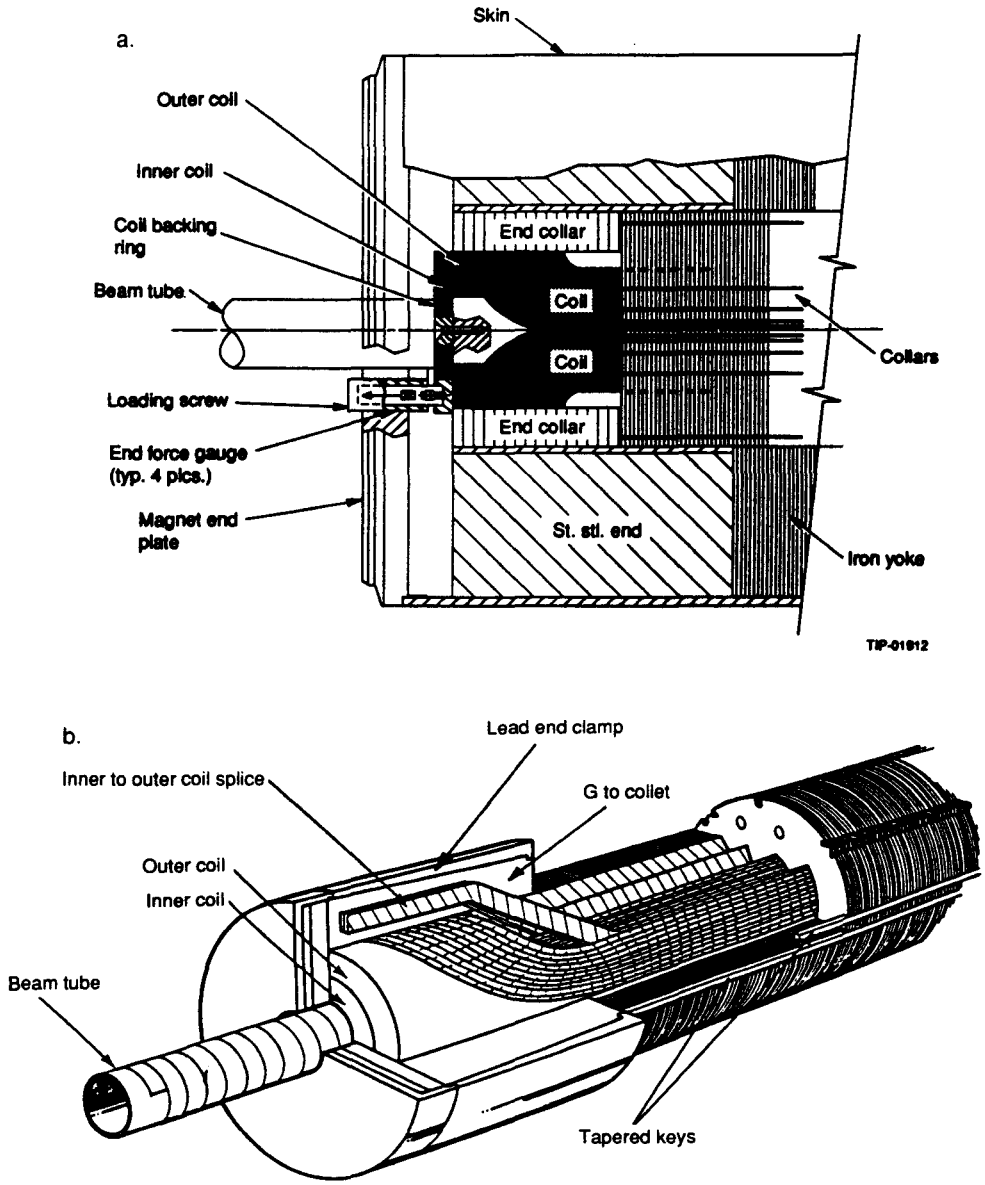

Figure 2. Cutaway view of the non-lead end part of 5-cm-aperture, 15-m-long dipole magnet prototype: (a) BNL, horizontally-split yoke, and (b) FNAL, vertically-split yoke dipole magnet designs.

FNAL Design

Figure 1(b) displays a cross-sectional view of the FNAL 5-cm-aperture dipole magnet design. The key features of the FNAL design are vertically-split yoke and horizontally-ovalized, stainless steel collars. The inner boundary of the vertically-split yoke is a circle with a radius of 67.81 mm. The outer boundary of the horizontally-ovalized collars consists of the union of four circular arcs, extending respectively between –30° and +30° about the midplane, and between –60° and +60° about the pole axis.[18] The four arcs have the same radius, which is 0.01 mm larger than the yoke's inner radius. However, the centers of the

arcs extending between –30° and +30° about the midplane are shifted outward along the horizontal axis by 0.14 mm with respect to the yoke center, while the centers of the arcs extending between –60° and +60° about the pole axis are shifted downward along the axis by 0.46 mm with respect to the yoke center. As a result, the vertical outer diameter of the keyed collars (with no coil in them) is 900 μm smaller than the yoke inner radius, while there is a 300-μm interference along the horizontal diameter.

The rationale behind the FNAL design is as follows. During excitation, the support of the yoke is needed mainly to limit the collar deflections along the horizontal diameter, where the effect of the radial component of the Lorentz force is largest. One way to ensure that such support is provided is to design collars and yokes so that they are always in contact along the horizontal diameter. The problem, however, is that the integrated thermal expansion coefficient between room and liquid helium temperatures of Nitronic-40 stainless steel is smaller than that of low-carbon steel. To maintain contact during cooldown, one must thus start with a positive interference at room temperature. A positive collar-yoke interference along the horizontal diameter can be produced only by a vertically-split yoke.

The vertically-split yoke and the horizontally-ovalized collars are thus designed to ensure that there is always a suitable collar-yoke interference along the horizontal axis. The amount of horizontal collar-yoke interference at room temperature is determined in order to at least compensate for the cooldown shrinkage differentials. On the other hand, in order to assemble the vertically-split yoke, one must ensure that there is enough clearance between the collared-coil assembly and the yoke along the vertical diameter. As we have seen, the large pre-compression of the coil during collaring results in a large vertical deflection of the collared-coil assembly. Thus the collars' vertical diameter must be smaller than the yoke's inner diameter. The reduction in vertical diameter of the horizontally-ovalized collars is determined to at least compensate for the vertical deflection resulting from collaring. Table 1 summarizes the estimated horizontal collar-yoke interference at room temperature for the five FNAL magnets considered in this paper. As for the BNL magnets, the estimate is based on measurements of the collared-coil assembly diameters and assumes that the yoke midplane gap is closed. The quoted values appear very close to the design value.

The assembly process of the FNAL vertically-split yoke magnets is similar to that of the BNL horizontally-split yoke magnets. The main difference is the use of a press during the welding of the outer shell. The press is required in order to close the gap between the two yoke halves, which arises from the built-in collar-yoke interference along the horizontal diameter. As a result, the collared-coil assembly is tightly clamped inside the yoke and, toward the magnet ends, a large fraction of the axial component of the Lorentz force can be transmitted to the yoke and the outer shell. The axial pre-load of the FNAL magnets is set to a lower value than that of the BNL magnets, typically between 10 and 20 kN.

Other specific features of the FNAL design include external splices between the inner and outer layer conductors, located at a larger radius than that of the coil outer layer. As displayed in Figure 2(b), the coil ends are surrounded by a four-piece G10 collet,[19] which at the lead end houses the splices. Coil ends and collets are compressed radially by a tapered, aluminium cylinder that is hydraulically slid into position. The junction between the last collar pack of the magnet body and the collet assembly is located approximately 76 mm before the end of the straight section of the coil inner layer. The FNAL magnets do not incorporate cross-flow cooling.

Instrumentation

The BNL and FNAL magnet prototypes have the same basic instrumentation. It includes voltage taps to locate the quench origins,[20] beam-type strain-gauge transducers to measure the pressure exerted by the coil against the collar poles,[21] and bullet-type strain-gauge assemblies to measure the force exerted by the coil against the end plates.[21] The

FNAL magnets are instrumented with two strain-gauge packs, one at the minimum and one at the maximum azimuthal coil sizes; the BNL magnets have only one strain gauge pack, at the minimum azimuthal coil size. Both ends of the BNL magnets are instrumented with bullet gauges, while only the non-lead end of the FNAL magnets is instrumented. (The non-lead end is the magnet end opposite that where the current leads are located). Strain gauges are also mounted on the outer shell of the FNAL magnets to measure azimuthal stress.[22]

The test stands' interconnects of both the BNL and the FNAL facilities incorporate temperature sensors, and warm- and cold-pressure transducers. In the case of the BNL test facility, the helium inlet coincides with the lead-end of the magnets, while the connections are opposite at the FNAL test facility. Typical helium mass flow rates are 40 to 50 g/s at FNAL, and 140 to 150 g/s at BNL.

MECHANICAL PERFORMANCE

Expected Behavior During Excitation

As we described earlier, the Lorentz force has three main components: 1) an azimuthal component, which tends to compress the coil towards the midplane and to unload the collar pole; 2) a radial component, which tends to bend the collars outwardly with a maximum deflection at the midplane; and 3) an axial component, which tends to stretch the coil ends. During excitation, the pressure exerted by the coil against the collar poles is thus expected to decrease as a function of current squared, while the force exerted by the coil against the end plates is expected to increase. Let us now qualitatively discuss the differences in behavior that can be expected from the two magnet designs.

In the case of the FNAL magnets, collars and yoke are designed to be always in contact along the horizontal diameter. During excitation, the yoke provides a quasi-infinitely stiff support against the radial component of the Lorentz force, and the collars do not bend. The unloading of the collar pole thus results only from the compression of the coil under the azimuthal component of the Lorentz force.

In the case of the BNL magnets, the cooldown shrinkage differentials result in a gap between the collared-coil assembly and the yoke, which extends over a certain angle on both sides of the horizontal plane. During excitation, the collars do bend and the coil deflects accordingly, with a maximum displacement along the horizontal diameter. The arc length of the coil increases, resulting in a decrease of azimuthal compressive stress. The initial unloading of the coil from the collar pole thus results from two causes: 1) the compression of the coil under the azimuthal component of the Lorentz force, and 2) the bending of the coil under the radial component of the Lorentz force.

From the above discussions, the BNL magnets would be expected to exhibit a faster initial rate of unloading than do the FNAL magnets. However, as the current increases the collars of the BNL magnets keep deflecting along the horizontal diameter, eventually coming into contact with the yoke. As the contact occurs, the yoke provides the desired support against the radial component of the Lorentz force, and the additional bending moment disappears. For currents above the contact current, the unloading of the collar pole results only from the azimuthal component of the Lorentz force, and the BNL magnets should behave similarly to the FNAL magnets. After the fast initial unloading, we are thus expecting the pressure plots of the BNL magnets to exhibit a change in slope and to become parallel to those of the FNAL magnets.

As for the end force, we are also expecting the BNL magnets to exhibit a faster rate of increase as a function of current squared than do the FNAL magnets. One reason is that the BNL ends are pre-loaded axially to a much higher level and are thus much stiffer. Another reason is that due to the smaller collar-yoke interference, less of the axial component of the Lorentz force is shared by friction between the collared-coil assembly, the yoke, and the shell, and more is directly transmitted to the end-plates.

Comparison of Beam-Type Strain-Gauge Measurements

Cooldown and excitation data for the coil inner and outer layers are summarized in Tables 2 and 3. The quoted values are an average over the four quadrants of the strain gauge packs. In the case of the FNAL magnets, which have two strain gauge packs, the data are differentiated by means of the letters LE and NLE, which refer to the location of the strain gauge pack with respect to the magnet ends.

Figure 3(a) presents a summary plot of the inner layer pressure as a function of current squared for the three BNL magnets, and Figure 3(b) presents a similar plot for the five FNAL magnets. The data displayed in Figure 3 were taken during strain-gauge runs performed after the quench plateau had been established. For each magnet, the pressures are averaged over the four quadrants of a selected strain-gauge pack, and only current up-ramp data are displayed. As expected, the initial rate of unloading of the BNL magnets appears to be faster than that of the FNAL magnets. Also, as the current increases, the traces of the BNL magnets flatten and become more nearly parallel to those of the FNAL magnets. However, none of the magnets presented here exhibit a complete unloading of the collar poles as was observed on some of the BNL 4-cm-aperture prototypes.[10]

Table 2. Summary of inner coil stress measurements on selected 5-cm-aperture, 15-m-long collider dipole magnet prototypes. The number and the number in parentheses correspond respectively to the mean and the standard deviation over the four quadrants of the given strain-gauge pack.

Magnet Name	Before First Cooldown (MPa)	After First Cooldown (MPa)	Before First Warmup (MPa)	Initial Stress vs. I^2 Slope (MPa/kA^2)[a]
DCA207	77 (5)	49 (6)	39 (4)	–1.02 (.08)
DCA208	69 (9)	36 (11)	29 (10)	–0.86 (.16)
DCA209	66 (2)	40 (4)	35 (4)	–0.92 (.02)
DCA311 (LE)	53 (8)	31 (8)	35 (9)	–0.71 (.08)
DCA311 (NLE)	52 (4)	32 (1)	40 (3)	–0.76 (.04)
DCA312 (LE)	91 (9)	59 (4)	61 (5)	–0.80 (.05)
DCA312 (NLE)	58 (4)	33 (5)	34 (4)	–0.62 (03)
DCA313 (LE)	63 (9)	44 (4)	46 (5)	–0.64 (.04)
DCA313 (NLE)	59 (4)	48 (5)	34 (5)	–0.65 (.04)
DCA314 (LE)	77 (3)			
DCA314 (NLE)	66 (9)	33 (8)	33 (8)	–0.66 (.11)
DCA315 (LE)	61 (5)	36 (4)	34 (4)	–0.58 (.03)
DCA315 (NLE)	53 (16)	31 (11)	21 (14)	–0.45 (.15)

[a] For a strain-gauge run performed after the quench plateau was established.

Table 3. Summary of outer coil stress measurements on selected 5-cm-aperture, 15-m-long collider dipole magnet prototypes. The number and the number in parentheses correspond respectively to the mean and the standard deviation over the four quadrants of the given strain-gauge pack.

Magnet Name	Before First Cooldown (MPa)	After First Cooldown (MPa)	Before First Warmup (MPa)	Initial Stress vs. I^2 Slope (MPa/kA^2)[a]	Contact Current (A)[a]
DCA207	55 (11)	27 (11)	22 (7)	–0.34 (.08)	4500
DCA208	69 (10)	39 (11)	36 (9)	–0.53 (.13)	4000
DCA209	64 (10)	34 (11)	31 (12)	–0.34 (.09)	4000
DCA311 (LE)	45 (9)	26 (4)	27 (4)	–0.18 (.09)	n/a
DCA311 (NLE)					n/a
DCA312 (LE)	36 (14)	30 (11)	20 (11)	–0.11 (.06)	n/a
DCA312 (NLE)	47 (25)				n/a
DCA313 (LE)	73 (14)	48 (11)	57 (26)	–0.19 (.06)	n/a
DCA313 (NLE)	59 (25)	34 (28)	33 (19)	–0.13 (.03)	n/a
DCA314 (LE)	56 (12)	50 (19)	50 (19)	–0.20 (.03)	n/a
DCA314 (NLE)	42 (3)	36 (20)	34 (21)	–0.18 (.05)	n/a
DCA315 (LE)	43 (14)				n/a
DCA315 (NLE)	28 (13)	15 (8)	15 (7)	–0.11 (.02)	n/a

[a] For a strain-gauge run performed after the quench plateau was established.

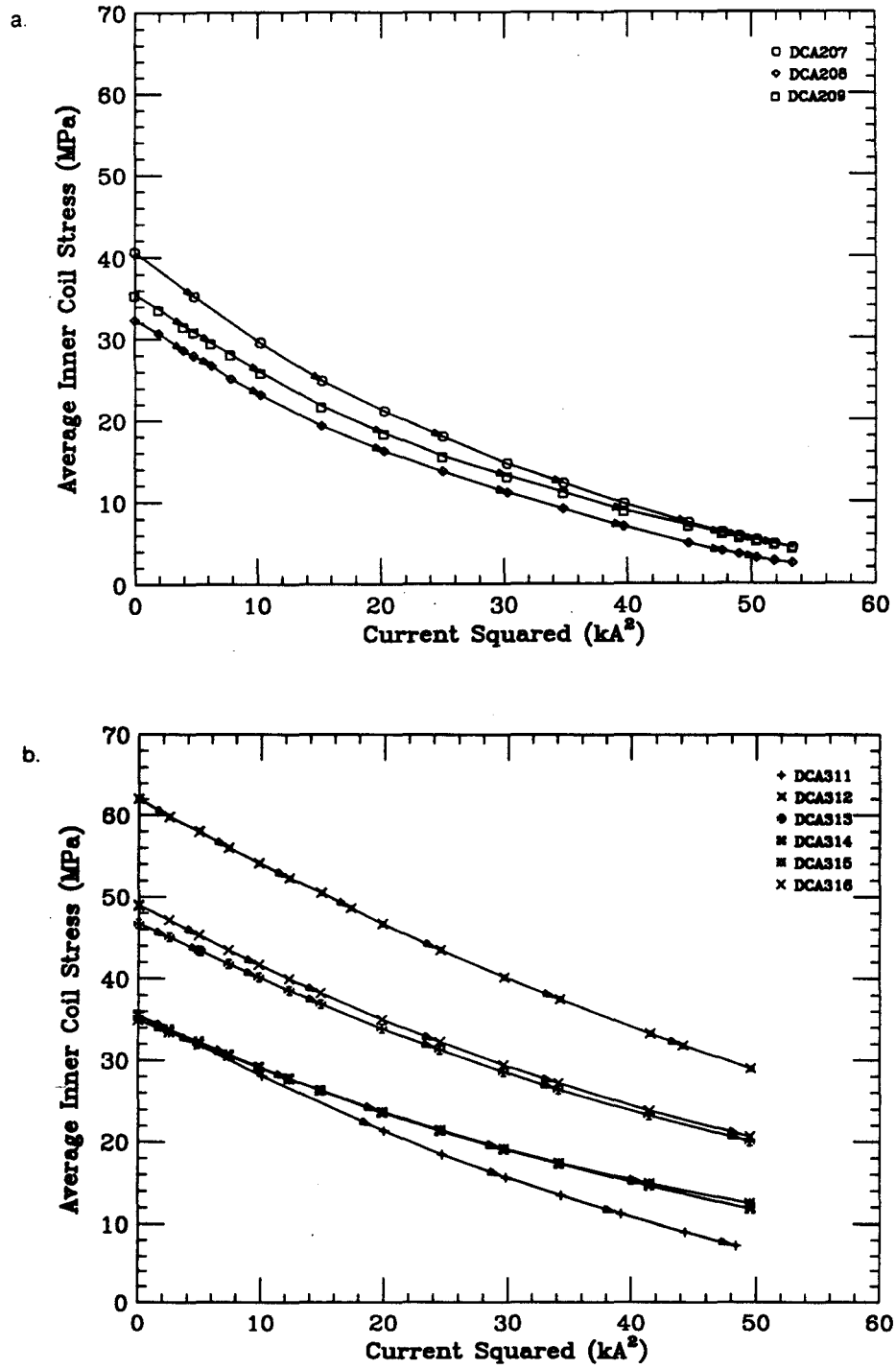

Figure 3. Summary of the changes in the azimuthal pressure exerted by the coil inner layer against the collar pole during excitations of the 5-cm-aperture, 15-m-long dipole magnet prototypes: (a) BNL, horizontally-split yoke, and (b) FNAL, vertically-split yoke dipole magnet prototypes. The pressure data are averaged over the four quadrants of selected strain gauge packs.

Let us discuss in more detail the initial slope of the pressure versus current squared. As we described, the unloading of the collar pole results from the Lorentz load on the coil. The Lorentz load is the same magnet to magnet, but what varies are the azimuthal stiffness of the coil and the radial stiffness of the collars. We have already explained what to expect for the collars' radial stiffness. On the other hand, the mechanical properties of the coil are known to be non-linear: the higher the stress, the stiffer the coil. Within each design family, we can thus expect the initial slope of the pressure versus current squared to be an increasing function of the coil pre-compression. Figure 4 presents a summary plot of the initial slopes of the inner-layer pressure versus current squared as a function of the inner-layer pressure at zero current. As expected, the magnets appear to lie on two lines with a positive slope: one for the FNAL magnets at the bottom of the plot, and one for the BNL magnets at the top of the plot.

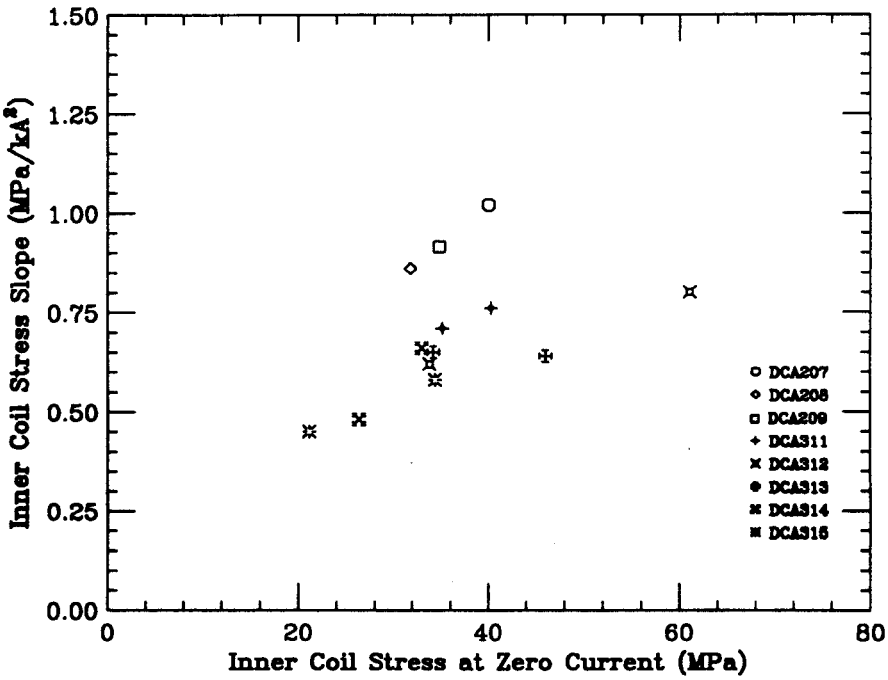

Figure 4. Correlation between the initial slopes of the inner-layer pressure versus current squared as a function of the pressures at zero current for the 5-cm-aperture, 15-m-long dipole magnet prototypes. The pressure data are averaged over the four coil quadrants.

Figure 5 presents summary plots of the outer-layer pressure as a function of current squared for the three BNL magnets and the five FNAL magnets. These measurements were taken during the same strain-gauge run as that of Figure 3. For each magnet the pressures are averaged over the four coil quadrants, and only the current up-ramp data are displayed. As with the inner-layer pressure, the initial rate of unloading of the BNL magnets appears to be faster than that of the FNAL magnets. As was also observed on the 4-cm-aperture prototypes,[10] the traces of the BNL magnets exhibit a clear change of slope for a current of about 4000 A. This current is interpreted as the current at which the collared-coil assembly comes into contact with the yoke along the horizontal diameter.

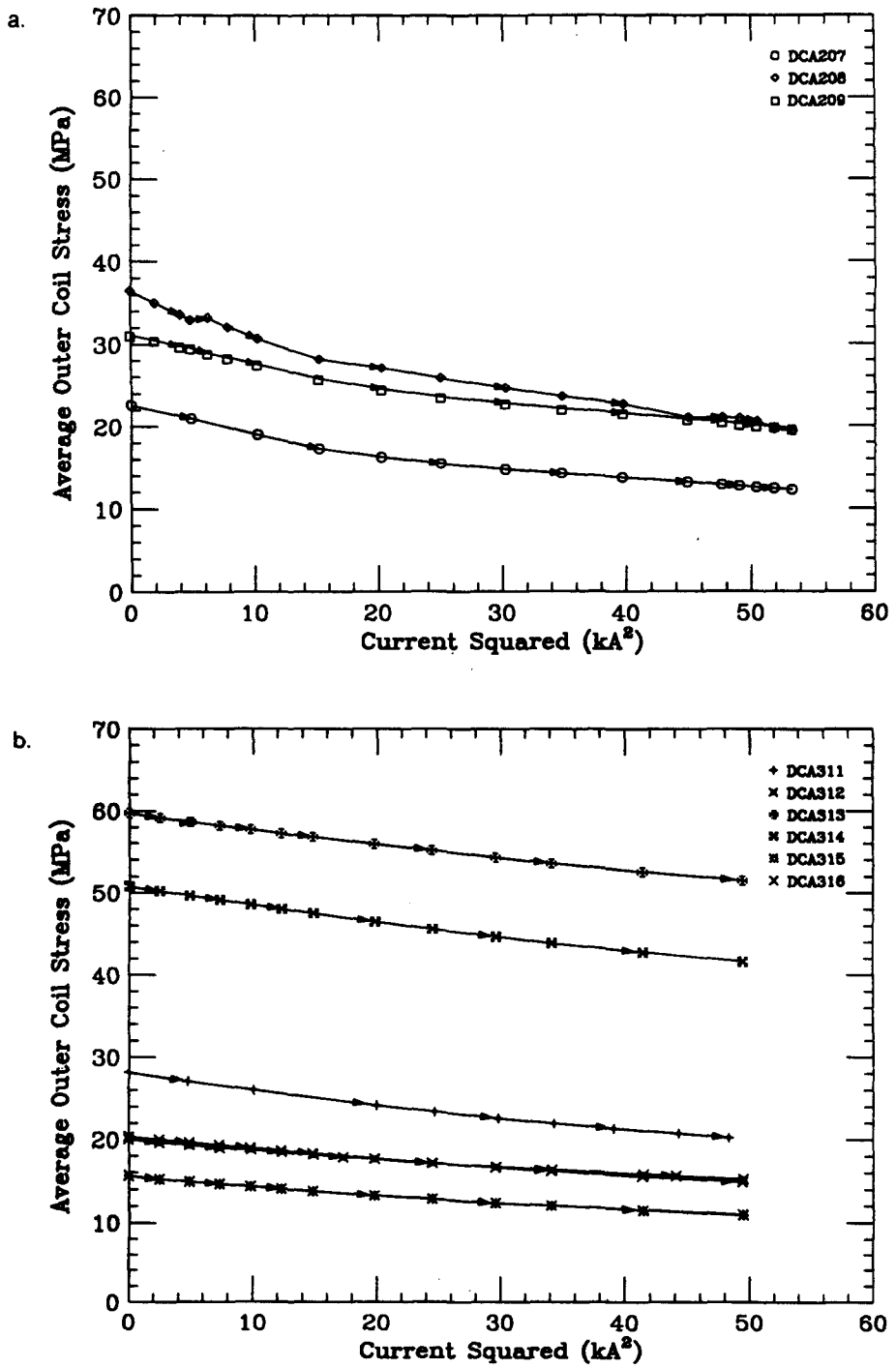

Figure 5. Summary of the changes in the azimuthal pressure exerted by the coil outer layer against the collar pole during excitations of the 5-cm-aperture, 15-m-long dipole magnet prototypes: (a) BNL, horizontally-split yoke, and (b) FNAL, vertically-split yoke dipole magnet prototypes. The pressure data are averaged over the four quadrants of selected strain gauge packs.

Comparison of End-Force Measurements

Figures 6 and 7 present plots of the end-force versus time during the testing of BNL magnet prototype DCA209 and FNAL magnet prototype DCA312. Each testing included two cycles separated by a warm-up to room temperature. Magnet DCA209 was equipped with bullet gauges at both ends. Data in Figure 6(a) are summed over the four lead-end bullet gauges, while data in Figure 6(b) are summed over the four non-lead-end bullet gauges. Magnet DCA312 was equipped only with bullet gauges at the non-lead end. Each arrow on the plots corresponds to an excitation above 1000 A, while each arrow with a number corresponds to a quench.

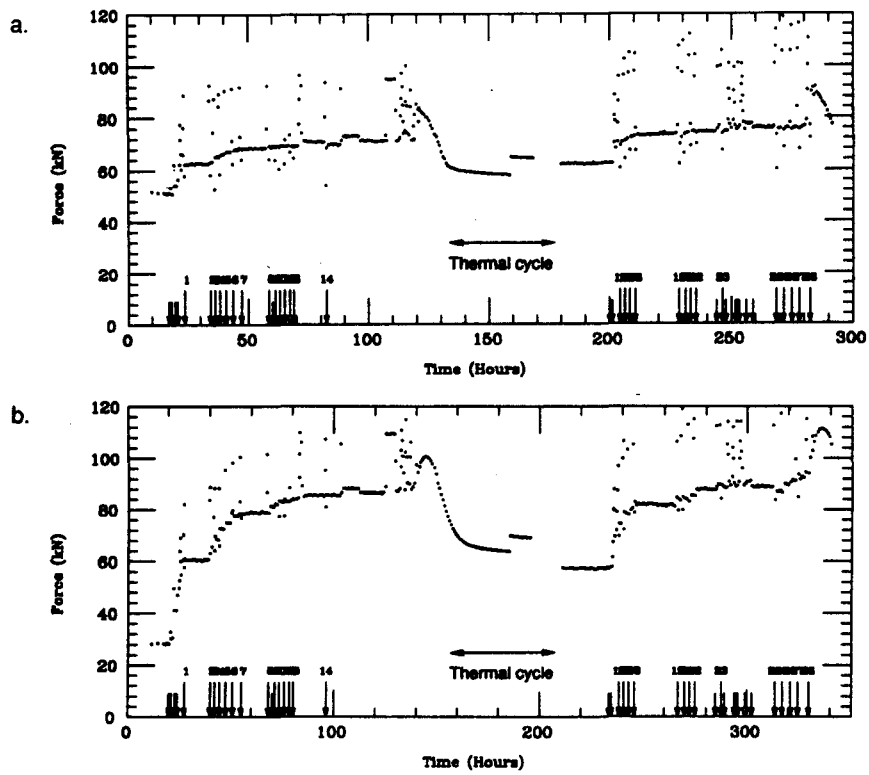

Figure 6. Change in the coil axial compressive loads during the testing of BNL 5-cm-aperture, 15-m-long dipole magnet prototype DCA209: (a) at the magnet lead end, (b) at the magnet non-lead end. The data are summed over the four loading screws of the given end. The small arrows indicate magnet excitations to a current larger than 1000 A. The large arrows surmounted by a number correspond to a quench.

The most striking difference between Figures 6 and 7 is that magnet DCA312 end-force appears to be quite stable, while that of magnet DCA209 appears to increase significantly over each of the testing cycles: the lead end gained 22 kN during the first testing cycle and 15 kN during the second, while the non-lead end gained 61 kN during the first testing cycle and 35 kN during the second. As can be seen in Figure 6, most of the increase takes place at the time of the first excitations after cooldown. It also appears that the warm-up to room temperature resets the end-force to a level similar to that prior to the first cooldown, and that the overall increase during the second cycle is somewhat less than that during the first cycle.

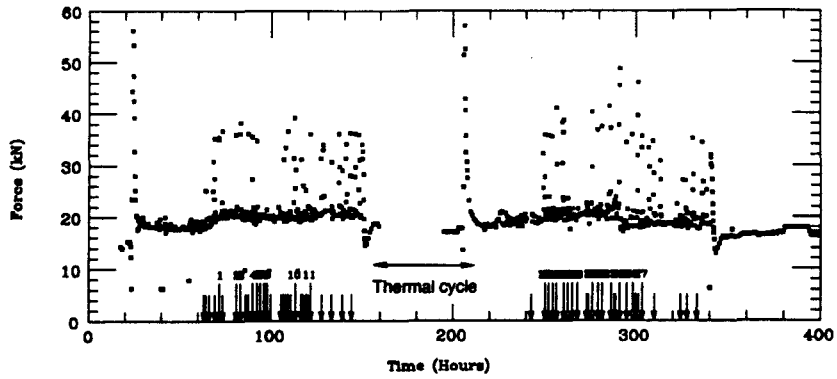

Figure 7. Change in the coil axial compressive load during the testing of FNAL 5-cm-aperture, 15-m-long dipole magnet prototype DCA312. The data are summed over the four loading screws at the magnet non-lead end. The small arrows indicate magnet excitations to a current larger than 1000 A. The large arrows surmounted by a number correspond to a quench.

The behaviors of magnets DCA209 and DCA312 that we just described are representative of the behaviors of the other magnets of the same design. Table 4 summarizes the end-force data for the eight magnets described in this paper. The quoted values are sums over the four bullet gauges of each end. It appears that the end-force of the FNAL magnets is always quite stable, while the end-force of the BNL magnets always exhibits a large increase over each of the testing cycles. This increase also appears to be always asymmetric, with the non-lead end gaining more than the lead end.

The origin of the end-force build-up, which was also observed on the BNL 4-cm-aperture prototypes,[10] is not yet fully understood. One possible explanation is a ratcheting of the collared-coil assembly inside the yoke. As we described, the axial component of the Lorentz force tends to pull the coil ends outwardly. A fraction of this axial component is transmitted to the end plate, but, for the most part, it is shared by friction between the collared-coil assembly, the yoke, and the shell. However, the contact surface between the laminated collars and the laminated yoke is very rough. Thus it can happen that as the current is ramped-up, or due to the thermal expansion following a quench, some collar laminations slip from one yoke lamination to the other, and that as the current is ramped-down or the magnet temperature is brought back to normal, these collar laminations stick to their new positions. These stick-slip motions could eventually explain the incremental increases of end-force during the first excitations or quenches.

It now remains to explain why the BNL magnets exhibit such behavior while the FNAL magnets do not. If the model of ratcheting is correct, the explanation could reside in the fact that the FNAL magnets have a larger collar-yoke interference than the BNL magnets. This larger collar-yoke interference results in a tighter clamping of the collared-coil assembly, eventually reducing the risks of stick-slip motions during excitation. As we shall see in the next section, however, the end-force ratcheting does not seem to have any impact on the quench performance of the BNL magnets.

Figure 8(a) presents a summary plot of the non-lead end-force as a function of current squared for the three BNL magnets, while Figure 8(b) presents a similar plot for the five FNAL magnets. These measurements were taken during the same strain-gauge runs as those of Figures 3 and 5—that is, after most of the ratcheting of the BNL magnets had occurred. For each magnet, the force is summed over the four bullet gauges at the non-lead end, and only the current up-ramp data are displayed. As expected, the BNL magnets exhibit a much faster rate of increase than the FNAL magnets, which is consistent with our understanding of the collar-yoke interference. (The difference in behavior between FNAL magnet DCA311 and the other FNAL magnets may be related to discrepancies in the yoke stacking and end-part assembly.)

Table 4. Summary of end-force measurements on selected 5-cm-Aperture, 15-m-long collider dipole magnet prototypes. The number and the number in parentheses correspond respectively to the sum and the standard deviation from the mean for the four bullet gauge assemblies of the given end.

Magnet Name	Before First Cooldown (kN)	After First Cooldown (kN)	Before First Warmup (kN)	After Second Cooldown (kN)	Before Second Warmup (kN)	Initial Force vs. I^2 Slope (kN/kA^2)[a]
DCA207 (LE)	64 (1.8)	54 (1.6)	62 (1.0)	56 (1.4)	60 (1.0)	0.5 (.01)
DCA207 (NLE)	68 (1.4)	66 (1.3)	92 (1.3)	74 (1.3)	91 (1.7)	0.6 (.01)
DCA208 (LE)	45 (1.2)	51 (1.2)	59 (1.2)	59 (1.4)	66 (1.5)	0.6 (.01)
DCA208 (NLE)	54 (0.9)	47 (0.9)	68 (0.9)	61 (1.1)	70 (1.0)	0.5 (.01)
DCA209 (LE)	44 (0.9)	51 (1.1)	73 (1.2)	62 (1.0)	77 (1.0)	0.6 (.00)
DCA209 (NLE)	29 (0.9)	28 (1.0)	88 (1.8)	57 (1.6)	92 (2.4)	0.5 (.01)
DCA311	20 (0.2)	33 (0.9)	33 (1.0)	32 (0.9)	34 (0.1)	0.13 (.01)
DCA312	14 (0.2)	18 (0.4)	20 (0.4)	19 (0.4)	18 (0.5)	0.3 (.02)
DCA313	22 (0.7)	29 (1.0)	26 (1.0)	26 (1.0)	29 (1.0)	0.4 (.02)
DCA314	18 (2.0)	17 (1.4)	20 (1.5)	18 (1.4)	22 (1.5)	0.3 (.02)
DCA315	9 (0.3)	13 (0.4)	12 (0.4)	12 (0.3)	11 (0.5)	0.2 (.01)

[a] For a strain-gauge run performed after the quench plateau of the first testing cycle was established.

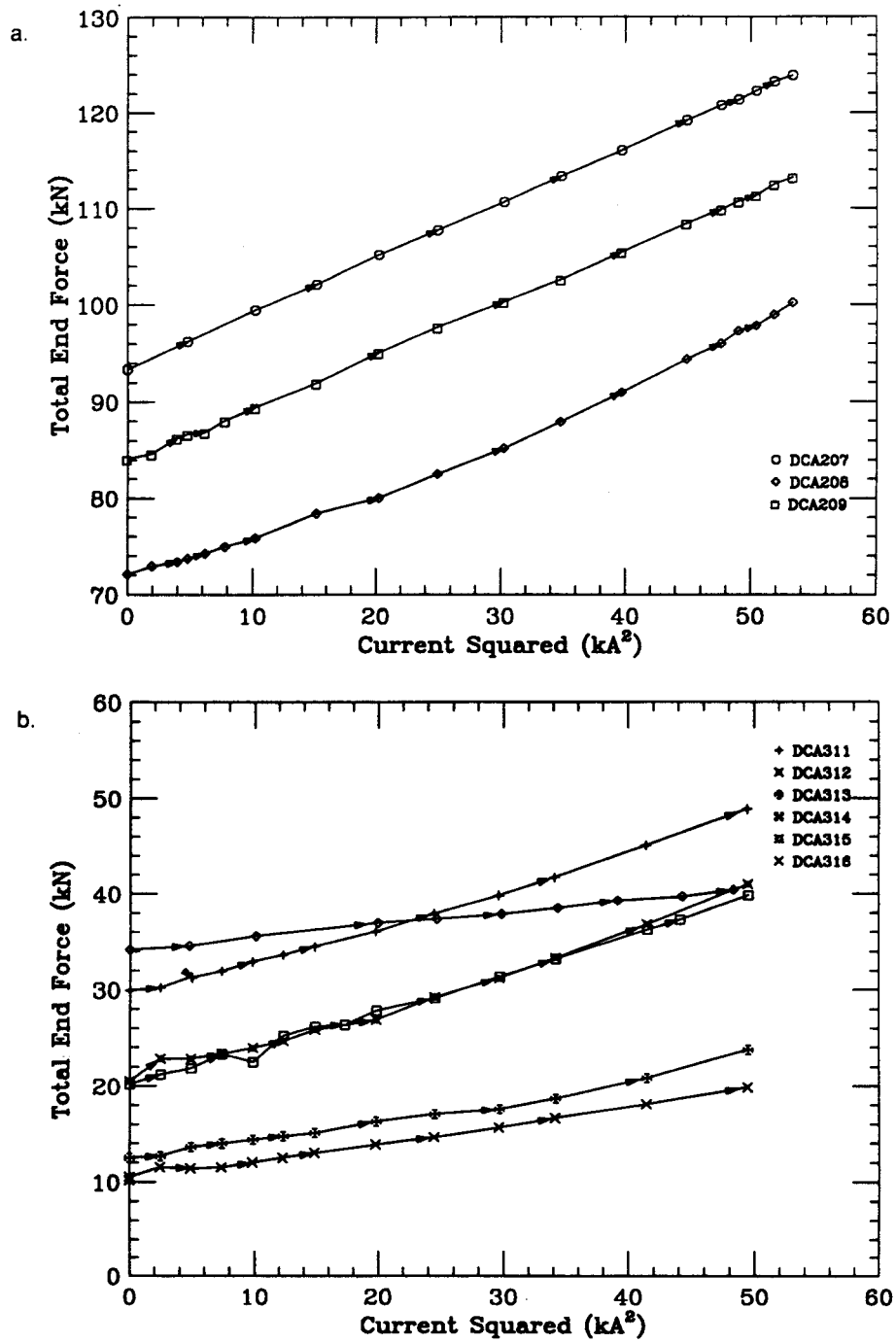

Figure 8. Summary of the changes in the axial force exerted by the coil against the end-plate loading screws during strain gauge runs performed after the establishment of a quench plateau for the 5-cm-aperture, 15-m-long dipole magnet prototypes: (a) BNL, horizontally-split yoke, and (b) FNAL, vertically-split yoke dipole magnet prototypes. The force data are summed over the four loading screws at the non-lead end of the magnets.

QUENCH PERFORMANCE

With the exception of BNL magnet DCA208, all the magnets were tested following the same run plan. The run plan calls for two testing cycles, separated by a warm-up to room temperature. The first cycle includes quench testing at 4.35 K and ramp-rate study. The second cycle includes quench testing at 4.35 K, 3.85 K, and 3.5 K. Due to schedule constraints, magnet DCA208 was not tested at low temperatures. At FNAL, the magnets are cooled down as rapidly as the cryogenic system allows; it takes about 24 hours. At BNL, up to and including the first cooldown of magnet DCA209, the magnets were cooled down in such a way that the temperature difference between the magnet ends would not exceed 50 K, increasing the cooldown time to about 36 hours. This restriction was removed during the second cooldown of DCA209 in order to match the cooldown time of the FNAL magnets.

Figure 9(a) presents a summary plot of the quench performance of the three BNL magnets, while Figure 9(b) presents a similar plot for the five FNAL magnets. The quenches reported here correspond to ramp rates less than or equal to 16 A/s, with the magnet bore tube evacuated. For all magnets, the first ramp to quench after the first cooldown is a strain gauge run, during which the current is increased in steps. For quenches 2 through 5 of the first testing cycle of FNAL magnet DCA311, the current was ramped at a rate of 16 A/s, while most of the other quenches on this magnet were approached at a ramp rate of 2 A/s. For subsequent magnets, the nominal current ramp was from 0 to 6500 A at 16 A/s, 10 min wait at 6500 A, and from 6500 A to quench at 4 A/s. Deviations from this nominal ramp include quenches 7 and 8 of the first testing cycle, and all the quenches of the second testing cycle of BNL magnet DCA209, for which the ramping from 6500 A to quench was performed at 1 A/s. The design ramp rate of the SSC collider ring is 4 A/s. The intermediate step at 6500A was introduced to remove the coil heating that results from the ramping at 16 A/s. Ramp-rate sensitivity will be discussed in the next section.

With the exception of the first quenches of FNAL magnets DCA313 and DCA314, the quench performance during the first testing cycle is quite satisfactory. BNL magnet DCA207 exhibited two training quenches, while BNL magnet DCA208 exhibited one, but they are all at currents above 7300 A. The first two quenches of BNL magnet DCA209 occurred respectively at 7100 A and 7305 A, while subsequent quenches were all above 7400 A. Note that this magnet exhibited a slight increase in quench current when the ramp rate was lowered from 4 A/s to 1 A/s. FNAL magnet DCA311 exhibited a similar trend when the ramp rate was lowered from 16 A/s to 4 A/s and 2 A/s, but it did not exhibit any noticeable training. Neither did FNAL magnets DCA312 and DCA315. The low-current quenches of FNAL magnets DCA313 and DCA314 occurred respectively at 4935 A and 5525 A, toward the lead end of the upper-inner quarter coil pole turn, on the side opposite the ramp splice. A missing voltage tap complicates the determination of the axial locations of these two quenches, but they appear to be similar and close to the boundary between the last collar pack of the magnet body and the lead-end collet. We speculate that they resulted from discrepancies in the assembly of the magnets' ends. After these first quenches, however, the magnets reached 7300 A, and the problem did not resurface.

The quench performance at 4.35 K after the thermal cycle is also quite satisfactory. BNL magnets DCA207 and DCA209 did not exhibit any noticeable retraining, while BNL magnet DCA208 exhibited one retraining quench at 7100 A. None of the FNAL magnets exhibited a noticeable retraining. With the exceptions of BNL magnet DCA209 and FNAL magnet DCA315, all the magnets went directly to plateau at 3.8 K. Magnets DCA209 and DCA315 both exhibited two training quenches (at 7745 A and 7920 A for magnet DCA209, and at 7660 A and 7815 A for magnet DCA315), and then reached plateau. All the magnets, except FNAL magnet DCA314, also reached plateau at 3.5 K, either directly (BNL magnet DCA207 and FNAL magnets DCA311, DCA313, and DCA315), or with a limited number

of training steps (BNL magnet DCA209 and FNAL magnet DCA312). The first quench of magnet DCA314 at 3.5 K occurred at 8320 A, which corresponds to the current limit that can be expected from the conductor used in this magnet (see below). The next two quenches, however, occurred respectively at 7985 A and 7710 A, and originated in the upper-outer quarter coil near the lead end. There was no further attempt to reach plateau. The lowest plateau at 3.5 K is that of FNAL magnet DCA311, with a current of 8100 A, corresponding to a force level 1.5 times larger than that at 6500 A. This demonstrates that the magnets of the two designs possess a large mechanical reserve.

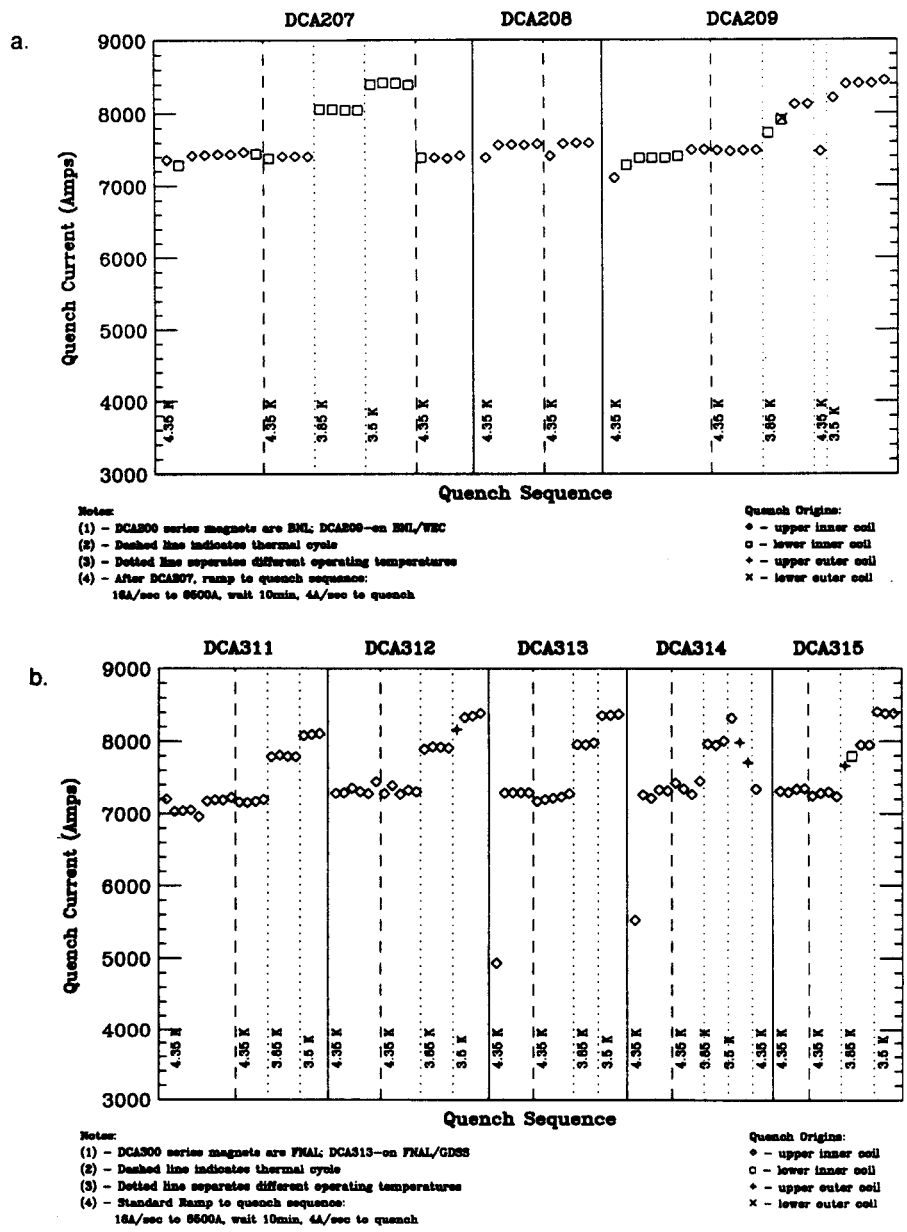

Figure 9. Summary of quench performance of 5-cm-aperture, 15-m-long dipole magnet prototypes: (a) BNL, horizontally-split yoke, and (b) FNAL, vertically-split yoke dipole magnet prototypes.

One interesting question to answer is how the plateau currents at the various temperatures compare to what can be expected from the known properties of the cables. Table 5 summarizes some of the parameters of the cables wound in these magnets, including the critical currents measured routinely at the BNL short-sample test facility. Figure 10 presents a summary plot of the highest plateau current at the given temperature as a function of the extrapolated short-sample current limit at the given temperature and field. The extrapolation is done using Green's parametrization of the NbTi critical surface.[23] Although most of the data points lie slightly below the first diagonal, the agreement is relatively good, indicating that the magnet assembly did not result in any significant degradation of the cable current capabilities. (It also indicates that the short sample extrapolations are quite reliable.)

Table 5. Selected parameters of inner cables wound in 5-cm-aperture, 15-m-long collider dipole magnet prototypes.

Magnet Name and Coil	Cable ID	Billet Number	Cu:NbTi	I_c at 4.22 K and 7 T (A)[a]	Cable RRR[a]	Coil RRR[b]
DCA207 Upper	SSC-3-I-00054	819-821	1.55	10904	39	220
DCA207 Lower	SSC-3-I-00055	819-822	1.54	10836	38	220
DCA208	SSC-3-I-00067	1096	1.34	11371	37	132
DCA209	SSC-3-O-00044	2594-7	1.50	11265	38	
DCA311	SSC-3-S-00023	2605	1.51	10079	37	175
DCA312 Upper	SSC-3-I-00047	819-822	1.53	10764	40	165
DCA312 Lower	SSC-3-I-00035	642	1.53	10673	42	167
DCA313	SSC-3-I-00052	822/857	1.52	10512	42	170
DCA314 Upper	SSC-3-I-00052	822/857	1.52	10512	42	174
DCA314 Lower	SSC-3-I-00049	819-822	1.52	10869	39	171
DCA315	SSC-3-I-00049	819-822	1.52	10869	39	170

[a] Measured on cable short sample.
[b] Measured on magnet during cold-testing.

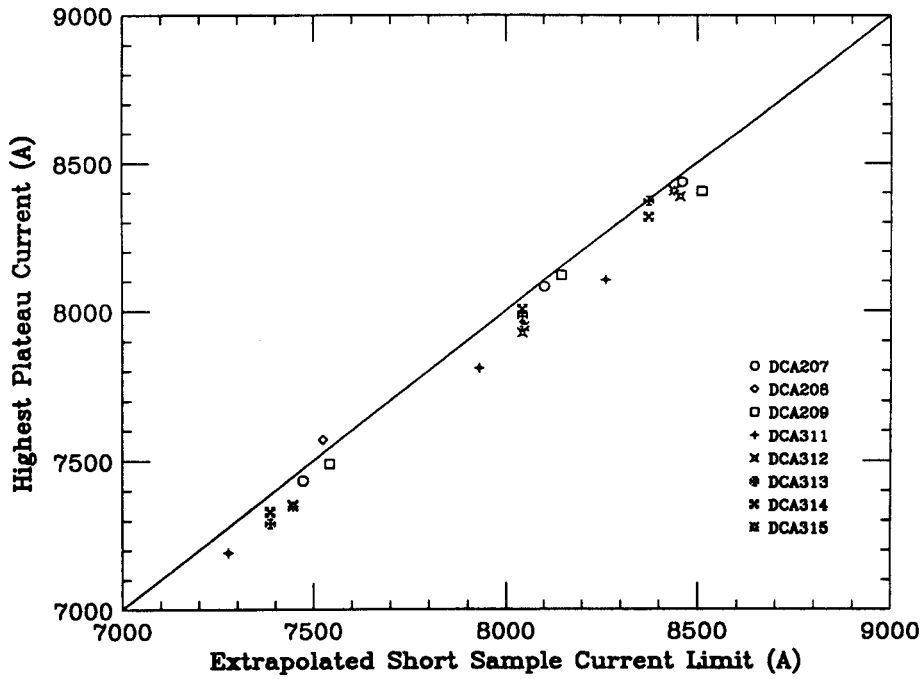

Figure 10. Comparison between quench plateau currents and short sample current limits extrapolated using Green's parametrization of the NbTi critical surface.

RAMP-RATE SENSITIVITY

When the current in a superconducting magnet is changed, heat is generated by several mechanisms: hysteresis in the superconductor and in the iron yoke, eddy currents flowing within the individual strands, and eddy currents flowing from strand to strand. The resultant temperature increase causes a decrease in the plateau current of the magnet, at a rate approximately equal to 20% per degree.

Figure 11 shows the decrease in quench current versus ramp rate for the eight magnets described in this paper. These magnets exhibit a far greater sensitivity to ramp rate than did earlier SSC dipole magnet prototypes, and it is believed that this can be attributed to unexpectedly large strand-to-strand eddy currents. This picture is supported by direct interstrand-resistance measurements performed at BNL on cable samples, showing that interstrand resistance is sometimes as much as two orders of magnitude smaller than expected.[24] Further, there appears to be a correlation between the decrease in quench current and the AC loss, as directly measured on some of the FNAL magnets.[25] In addition, as the ramp rate is increased, quench origin shifts from the pole turn, where the field is maximum, to the coil midplane, where the field is normal, to the wide face of the cable, producing the largest interstrand losses; this shift in location was predicted theoretically. In Figure 11, BNL magnets appear to be less sensitive than FNAL magnets. It is believed that this difference can be principally attributed to a difference in heat removal from the coil, as BNL magnets employ cross-flow cooling and are tested with a significantly higher mass-flow rate of helium.

There is as yet no clear explanation of why today's cables appear to be lossier than previous cables. Preliminary investigations reveal possible links to changes in processing of

the strand, cable, and coil that affect the RRR, ductility, and surface condition of the conductor. Note that although this sensitivity is of no concern to the operations of the SSC collider ring (with its nominal ramp rate of 4 A/s), it can be a problem for the high energy booster, which requires a ramp rate of the order of 70 A/s.

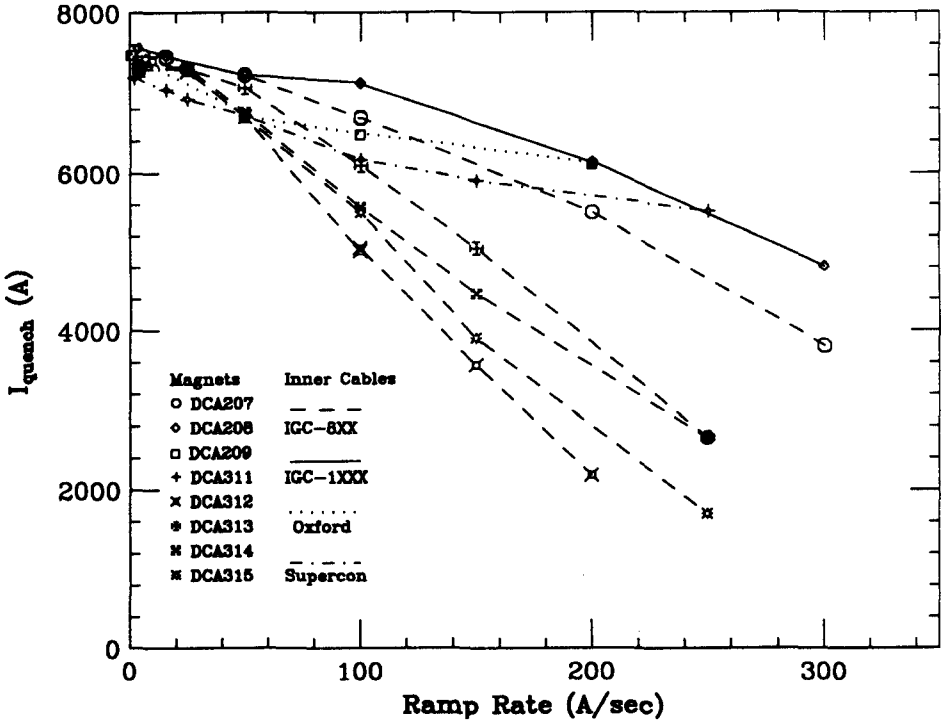

Figure 11. Summary of current at quench versus ramp rate for the 5-cm-aperture, 15-m-long dipole magnet prototypes.

CONCLUSION

The BNL and FNAL magnets perform according to their somewhat different mechanical designs, and they appear to be equally successful in terms of quench performance. The data from these magnets provide a sound basis for the dipole contractors to start their design effort. Aside from the ramp-rate sensitivity, the characteristics of the magnets are well understood, and the contractors can assess the operation of the two different designs under nominal conditions in developing a final product that is readily manufacturable and that meets all performance requirements, including those affecting its reliability.

ACKNOWLEDGMENTS

We are deeply indebted to M. Tigner, who laid out the SSC magnet R&D program and who, by heavily instrumenting the early magnet prototypes, envisioned the means of its success. We wish to thank V. Karpenko, who promoted the 4-cm-aperture design, and R. Palmer, who promoted the 5-cm-aperture design. We are also grateful to J. Peoples, Jr., who, by his charisma and determination, boosted the R&D efforts. This program, however, owes most of its success to the hard work and dedication of the teams at Brookhaven National Laboratory and Fermi National Accelerator Laboratory, who ensured the continuity of the magnet program and were instrumental in designing, building, and cold-testing the dipole magnet prototypes.

REFERENCES

1. J. D. Jackson, ed., "Conceptual Design of the Superconducting Super Collider," SSC-SR-1020, March 1986; revised, September 1988.
2. J. R. Sanford and D. M. Matthews, ed., "Site-Specific Conceptual Design of the Superconducting Super Collider," SSCL-SR-1056, July 1990.
3. T. Garavaglia, S. K. Kauffmann, and R. Stiening, "Collider Ring Particle Loss Tracking with SSCTRK," *Supercollider 2*, M. McAshan, ed., 1990, pp. 77–84.
4. K. Hosoyama, T. Shintomi, *et al.*, "Fabrication and Test of a 5-cm Aperture, 1-m Long SSC Collider Dipole Magnet," *Supercollider 3*, J. Nonte, ed., 1991, pp. 615–624.
5. J. Muratore, M. Anerella, *et al.*, "Construction and Test Results from 1.8-m-Long, 50-mm-Aperture SSC Model Collider Dipoles," to be published in these proceedings.
6. M. Lamm, R. Bossert, *et al.*, "Results from the Fermilab 1.5-m Model Magnet Program," to be published in these proceedings.
7. R. Gupta, S. A. Kahn, and G. H. Morgan, "SSC 50 mm Dipole Cross Section," *Supercollider 3*, J. Nonte, ed., 1991, pp. 587–599.
8. J. Strait, B. C. Brown, *et al*, "Tests of Full Scale SSC R&D Dipole Magnets," *IEEE Trans. Magn.*, **25**, No. 2, 1989, pp. 1455–1458.
9. J. Tompkins, M. Chapman, *et al*, "Performance of Full-Length SSC Model Dipoles: Results from 1988 Tests," *Supercollider 1*, M. McAshan, ed., 1989, pp. 33–49.
10. A. Devred, T. Bush, *et al*, "About the Mechanics of SSC Dipole Magnet Prototypes," to be published in AIP Conference Proceedings Series, "The Physics of Particle Accelerators," 1992.
11. J. Strait, K. Coulter, *et al.*, "Experimental Evaluation of the Vertically Versus Horizontally Split Yokes for SSC Dipole Magnets," *Supercollider 2*, M. McAshan, ed., 1990, pp. 731–741.
12. M. Anerella, J. Cottingham, *et al.*, "Construction and Test Results from 15-m-Long, 50-mm-Aperture SSC Collider Dipole Models," to be published in these proceedings.
13. M. J. Blessing, D. E. Hoffman, *et al.*, "Construction Experience with Fermilab-Built Full-Length 50-mm SSC Dipoles," to be published in these proceedings.
14. P. Wanderer, M. Anerella, *et al.*, "A Summary of SSC Dipole Magnet Field Quality Measurements," to be published in these proceedings.
15. S. Delchamps, M. Bleadon, *et al.*, "Magnetic Field Measurements of Fermilab/General Dynamics Built Full Scale SSC Collider Dipole Magnets," to be published in these proceedings.
16. C. Peters, K. Mirk, *et al.*, "Use of Tapered Key Collars in Dipole Models for the SSC," *IEEE Trans. Magn.*, **24**, No. 2, 1988, pp. 820–822.
17. R. P. Schutt and M. L. Rehak, "Transverse Cooling in SSC Magnets," *Supercollider 1*, M. McAshan, ed., 1990, pp. 209–217.
18. J. Strait, J. Kerby, *et al.*, "Mechanical Design of the 2D Cross-section of the SSC Collider Dipole Magnet," *Proceedings of the 1991 IEEE Particle Accelerator Conference*, 1991, pp. 2176–2178.
19. P. Heger, R. Bossert, *et al.*, "Design and Construction Experience with Collet End Clamps for 50-mm Aperture SSC Collider Dipoles," to be published in these proceedings.
20. A. Devred, M. Chapman, *et al.*, "Quench Start Localization in Full-Length SSC R&D Dipoles," *Supercollider 1*, M. McAshan, ed., 1989, pp. 73–83.
21. C. L. Goodzeit, M. D. Anerella, *et al.*, "Measurement of Internal Forces in Superconducting Accelerator Magnets with Strain Gauge Transducers," *IEEE Trans. Magn.*, **25**, No. 2, 1989, pp. 1463–1468.
22. M. Wake, M. Bleadon, *et al.*, "Mechanical Behavior of Fermilab/General Dynamics Built 15-m SSC Collider Dipoles," to be published in these proceedings.
23. M.A. Green, "Calculating the J_C, B, T Surfaces for Niobium Titanium Using a Reduced-State Model," *IEEE Trans. Magn.*, **25**, No. 2, 1989, pp. 2119–2122.
24. A. Gosh, private communication.
25. J. Strait, D. Orris, *et al.*, "Quench Performance of Fermilab/General Dynamics Built Full Length SSC Collider Dipole Magnets," to be published in these proceedings.